APPLIED PHYSICS LETTERS VOLUME 81, NUMBER 4 22 JULY 2002

Pseudodielectric function of $ZnGeP_2$ from 1.5 to 6 eV

V. Blickle
Department of Physics, University of Konstanz, D-78457 Konstanz, Germany

K. Flock, N. Dietz, and D. E. Aspnes[a)]
Department of Physics, North Carolina State University, Raleigh, North Carolina 27695-8202

(Received 14 January 2002; accepted for publication 14 May 2002)

We report pseudodielectric function data $\langle\varepsilon\rangle=\langle\varepsilon_{a_1}\rangle+i\langle\varepsilon_{a_2}\rangle$ and $\langle\varepsilon\rangle=\langle\varepsilon_{c_1}\rangle+i\langle\varepsilon_{c_2}\rangle$ for the optically uniaxial material $ZnGeP_2$, critical point energies of structures in these data, and dielectric function data for the natural oxide. Annealing reduces the values of the peaks of $\langle\varepsilon_{a_2}\rangle$. © *2002 American Institute of Physics.* [DOI: 10.1063/1.1492022]

Zinc germanium diphosphide ($ZnGeP_2$) is an optically uniaxial ternary II–IV–V_2 semiconductor that crystallizes in the chalcopyrite structure. The material is particularly relevant for nonlinear optical applications, including frequency-doubling CO_2 laser radiation and for expected applications involving sum-frequency generation, four-wave mixing, etc. Thus, there is considerable interest in determining its properties, and in particular its optical properties. The first measurements of the above-band gap optical properties were made by de Alvarez *et al.*, who also presented the first calculations of the energy band structure of this material.[1] More refined band structure calculations were later published by others,[2,3] and calculated dielectric functions were presented in Refs. 1 and 4. Optical measurements also include studies of birefringence[5,6] and photoluminescence.[7,8] However, no direct measurements of the above-band gap dielectric properties have yet been performed.

Here, we present pseudodielectric function data $\langle\varepsilon_a\rangle=\langle\varepsilon_{a_1}\rangle+i\langle\varepsilon_{a_2}\rangle$ and $\langle\varepsilon_c\rangle=\langle\varepsilon_{c_1}\rangle+i\langle\varepsilon_{c_2}\rangle$ for $ZnGeP_2$ from 1.5 to 6.0 eV for the tensor components along the ordinary (a) and extraordinary (c) principal axes of the material. We obtain these data using spectroscopic ellipsometry (SE), taking advantage of the real-time capabilities of the approach to determine when overlayers have been removed as much as possible by chemical stripping and therefore to obtain what we believe to be the best representation so far of the intrinsic bulk dielectric response of the material. We also report the influence of annealing on $\langle\varepsilon_a\rangle$, since heat treating is known to improve the electronic properties of the material.[8] In addition, we use these data in connection with the $\langle\varepsilon_a\rangle$ data obtained before stripping to determine the dielectric response of the natural oxide over the same spectral range where $ZnGeP_2$ is optically absorbing.

Our data were obtained with an automatic rotating-analyzer SE that has been described elsewhere, and processed with data-reduction methods appropriate for quartz Rochon prisms.[9,10] Measurements were made at an angle of incidence of 67.08°. The samples were contained in a windowless cell in flowing dry N_2. This configuration allowed us to chemically strip the surfaces of oxide overlayers while assessing the effectiveness of the cleaning procedure in real time, a capability necessary for minimizing overlayer effects. It also prevented atmospheric contamination and oxide regrowth from occurring during and after chemical stripping.

We investigated specifically four $ZnGeP_2$ crystals grown by the horizontal Bridgman method. Two were annealed in vacuum at 500 °C for 400 h. The effects of annealing on optical absorption are described in Ref. 8. The annealed samples, of size 20×30 mm, were oriented with the c axis perpendicular to one of the large faces. The as-grown samples were smaller, 5×5 mm, and oriented with the c axis in the plane of the large faces. This orientation permitted independent measurements of both components of $\langle\varepsilon\rangle$ of this optical uniaxial material, since Ref. 11 showed theoretically and experimentally that for samples oriented with one principal axis normal to the surface and a second in the plane of incidence, to a very good approximation $\langle\varepsilon\rangle$ as measured by ellipsometry is the component of the dielectric tensor along the intersection of the surface and the plane of incidence. We established the direction of the c axis with reflectance-difference spectroscopy. Furthermore the alignment was checked during the calibration process.[9] If a principal axis is not in the plane of incidence then the calibration procedure yields an apparent polarizer azimuth for the plane of incidence that is different from the correct value. One large face of each sample was initially polished, then given a final polish with lens paper and a bromine–methanol solution. Further real-time cleaning experiments with water, methanol, bromine–methanol, and HF showed that the most abrupt surfaces, as established by the highest peak values of $\langle\varepsilon_2\rangle$, were obtained with a bromine–methanol rinse followed by a second rinse with de-ionized water.

Figures 1 and 2 show our best values of $\langle\varepsilon_a\rangle$ and $\langle\varepsilon_c\rangle$, respectively, which were obtained with the as-grown samples. Due to the lack of sensitivity of rotating-analyzer ellipsometry to small values of $\langle\varepsilon_2\rangle$, all $\langle\varepsilon_2\rangle$ data that were obtained below the absorption edges near 2.3 eV were replaced by zero, because the material is known to be transparent at these energies. The overall shapes of the two spectra are similar, with the main differences occurring in the fine structure resulting from transitions at critical points within the material. These differences are most noticeable at the E_1 and E_2 structures near 3.0 and 4.8 eV, respectively, in the diamond/zinc blende nomenclature for these features. In particular, the weightings of the two components of the E_1

[a)]Electronic mail: aspnes@unity.ncsu.edu

 © 2002 American Institute of Physics

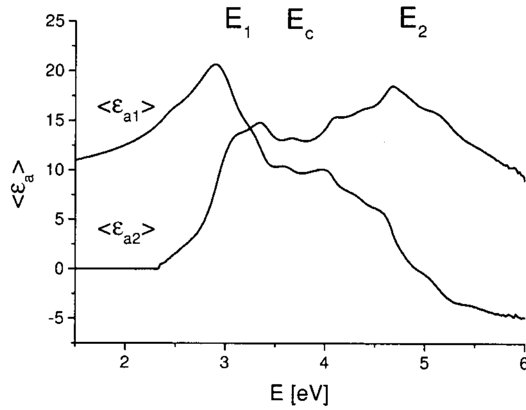

FIG. 1. Pseudodielectric function spectra obtained with the a axis parallel to both surface and plane of incidence for the as-grown sample with overlayers removed.

TABLE I. Critical point energies associated with different features in Figs. 1 and 2.

a axis		*c* axis	
Structure	CP energy (eV)	Structure	CP energy (eV)
Edge	2.45	Edge	2.35
Shoulder	3.00	Peak	2.88
Peak	3.39	Shoulder	3.12
Peak	3.58	Peak	3.68
Shoulder	4.07	Shoulder	4.19
Shoulder	4.38	⋯	⋯
Peak	4.67	Peak	4.61
Shoulder	5.12	⋯	⋯

structure are different for the a and c directions, and the E_2 feature for the c-axis spectrum shows two peaks instead of one. The absence in a given spectrum of features characteristic of the other spectrum provide a measure of our capability to separate the two components of the dielectric tensor.

From the band structure calculations of de Alvarez *et al.*,[1] we can assign the structures to the E_1, E_c, and E_2 critical points near 3.0, 3.6, and 4.8 eV respectively. However, it is our expectation that the present data will stimulate improved band structure calculations. As additional motivation and to provide information to assist in assessing the accuracy of these calculations, we determined the critical point energies associated with these features using a combination of direct- and reciprocal-space analysis. Reciprocal-space analysis has the advantage of being model independent since critical-point energies are determined independent of the actual direct-space line shapes. It also reveals when two singularities are too close to be resolved, as is the case for the features near 3 eV. The reciprocal-space results were confirmed with direct-space analysis on numerically calculated third derivatives of the line shapes with respect to energy. The critical point energies themselves are listed in Table I for both $\langle\varepsilon_a\rangle$ and $\langle\varepsilon_c\rangle$, with the features described qualitatively and those of probable common origin appearing in the same row. Estimated uncertainties do not exceed 20 meV, and for some values are less. The method of analysis and other aspects will be described elsewhere.

Results of annealing are shown in Fig. 3. Here, we compare the spectrum of Fig. 1 with $\langle\varepsilon_a\rangle$ data obtained on one of the samples heat treated as described earlier. The differences are minor. The E_1 peak in $\langle\varepsilon_{a_2}\rangle$ is about 5% lower, and the as-grown structures are somewhat sharper. We attribute this to outdiffusion of Zn during the annealing process.

To determine the dielectric properties ε_o of the natural oxide, we analyzed the $\langle\varepsilon_{a_2}\rangle$ data obtained before oxide removal with the reference data shown in Fig. 1. We determined the thickness d and ε_o independently using the method of Arwin *et al.*[12,13] Specifically, we write the formal solution of the three-phase (substrate/overlayer/ambient) model on a wavelength-by-wavelength basis as $\varepsilon_o = \varepsilon_l(\langle\varepsilon\rangle,\varepsilon_s,d_0,\ldots)$ where ε_s is the dielectric function of the substrate and d_0 is the exact thickness. If our estimate d of d_0 is not correct the result is

$$\varepsilon_o+\Delta\varepsilon_o=\varepsilon_o(\langle\varepsilon\rangle,\varepsilon_s,d,\theta,\ldots)\approx\varepsilon_o(\langle\varepsilon\rangle,\varepsilon_s,d_0,\theta,\ldots) + (d-d_0)\frac{\partial\varepsilon_o}{\partial d}. \quad (1)$$

Although we do not know ε_o *a priori*, we do know that, as an oxide, it cannot contain structure related to that of ε_s. For this sample the substrate contribution vanishes only for $d = d_0 = 29$ Å, which results in the ε_o spectrum shown in Fig. 4. The irregularities in these data are artifacts resulting from a combination of causes including the use of an oversimplified model, reference data that may also contain residual overlayer effects, and experimental uncertainties including noise. The true dielectric response of the oxide is expected to be slowly varying with energy, and could be represented more accurately, for example, by a Sellmeier fit to these data.

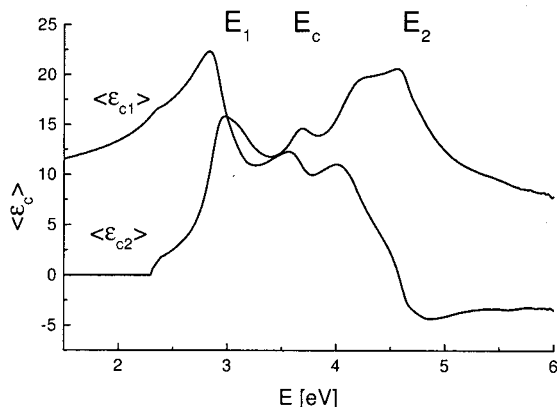

FIG. 2. As Fig. 1 but with the c axis so oriented.

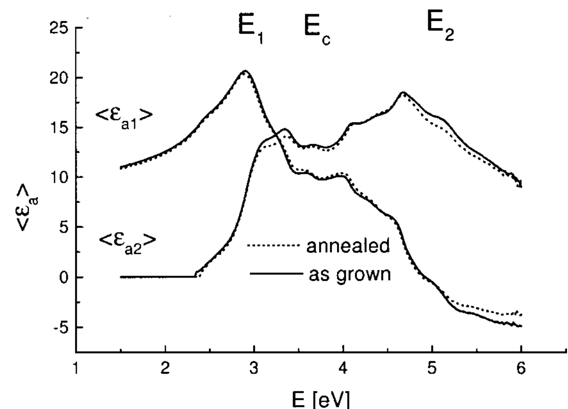

FIG. 3. $\langle\varepsilon_a\rangle$ for the annealed and as-grown $ZnGeP_2$ crystals.

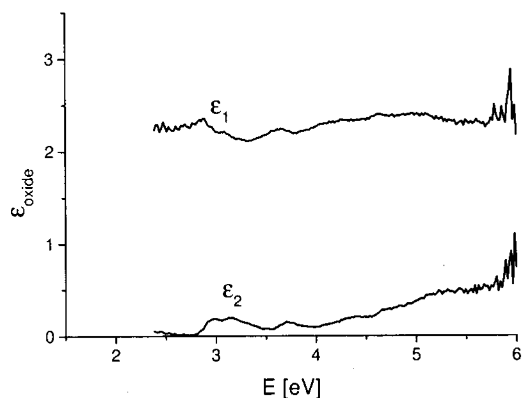

FIG. 4. The dielectric function of the natural oxide layer above the band gap of $ZnGeP_2$. The thickness of the oxide layer is 29 Å.

The results are reasonable, being similar to those obtained for the anodic oxide on the related compound GaP.[14,15] The dielectric function of the anodic oxide of GaP is smaller than those of the anodic oxides of GaAs and GaSb. The oxide of $ZnGeP_2$ is smaller than that of GaP by about 20%. Further, the $ZnGeP_2$ oxide shows only a small, fairly broad absorption edge in our spectral range, making it more nearly like that of the oxide of GaP, which is essentially transparent over this entire spectral range. In contrast, the oxides of GaAs and GaSb show strong absorption thresholds at 5.0 and 4.2 eV, respectively.

The authors are pleased to acknowledge support of this work from the Office of Naval Research and an Award for International Cooperation from the Max-Planck-Gesellschaft. The authors also thank G. D. Powell for useful technical discussions.

[1] C. V. de Alvarez, M. L. Cohen, S. E. Kohn, Y. Petroff, and Y. R. Shen, Phys. Rev. B **10**, 5175 (1974).
[2] S. Limpijumnong, W. R. L. Lambrecht, and B. Segall, Phys. Rev. B **60**, 8087 (1999).
[3] J. E. Jaffe and A. Zunger, Phys. Rev. B **30**, 741 (1984).
[4] S. N. Rashkeef, S. Limpijumnong, and W. R. L. Lambrecht, Phys. Rev. B **59**, 2737 (1999).
[5] D. W. Fischer and M. C. Ohmer, J. Appl. Phys. **77**, 5942 (1995).
[6] D. W. Fischer and M. C. Ohmer, J. Appl. Phys. **81**, 425 (1996).
[7] G. K. Averkieva, I. A. Maltseva, V. D. Prochukhan, and Y. V. Rud, Phys. Status Solidi A **39**, 453 (1977).
[8] N. Dietz, I. Tsveybak, W. Rudermann, G. Wood, and K. J. Bachmann, Appl. Phys. Lett. **65**, 2759 (1994).
[9] D. E. Aspnes and A. A. Studna, Appl. Opt. **14**, 220 (1975).
[10] D. E. Aspnes, J. Opt. Soc. Am. **64**, 812 (1974).
[11] D. E. Aspnes, J. Opt. Soc. Am. **70**, 1275 (1980).
[12] H. Arwin and D. E. Aspnes, Thin Solid Films **138**, 196 (1986).
[13] H. Arwin and D. E. Aspnes, Thin Solid Films **113**, 101 (1984).
[14] S. Zollner, Appl. Phys. Lett. **63**, 2523 (1993).
[15] D. E. Aspnes, B. Schwartz, A. A. Studna, L. Derick, and L. A. Koszi, J. Appl. Phys. **48**, 3510 (1977).